Displacement in the parameter space versus spurious solution of discretization with large time step



2004 J. Phys. A: Math. Gen. 37 1203

(http://iopscience.iop.org/0305-4470/37/4/008)

INSTITUTE OF PHYSICS PUBLISHING JOURNAL OF PHYSICS A: MATHEMATICAL AND GENERAL

J. Phys. A: Math. Gen. **37** (2004) 1203–1218 PII: S0305-4470(04)63715-2

# Displacement in the parameter space versus spurious solution of discretization with large time step

**Eduardo Mendes**[1] **and Christophe Letellier**[2]

[1] Laboratório de Modelagem, Análise e Controle de Sistemas Não Lineares, Universidade Federal de Minas Gerais, Av. Antônio Carlos 6627, 31270-901 Belo Horizonte, MG, Brazil
[2] Groupe d'Analyse Topologique et de Modélisation de Systèmes Dynamiques, Université de Rouen—CORIA UMR 6614, Av. de l'Université, BP 12, F-76801 Saint-Etienne du Rouvray Cedex, France

Received 15 May 2003
Published 9 January 2004
Online at stacks.iop.org/JPhysA/37/1203 (DOI: 10.1088/0305-4470/37/4/008)

**Abstract**

In order to investigate a possible correspondence between differential and difference equations, it is important to possess discretization of ordinary differential equations. It is well known that when differential equations are discretized, the solution thus obtained depends on the time step used. In the majority of cases, such a solution is considered spurious when it does not resemble the expected solution of the differential equation. This often happens when the time step taken into consideration is too large. In this work, we show that, even for quite large time steps, some solutions which do not correspond to the expected ones are still topologically equivalent to solutions of the original continuous system if a displacement in the parameter space is considered. To reduce such a displacement, a judicious choice of the discretization scheme should be made. To this end, a recent discretization scheme, based on the Lie expansion of the original differential equations, proposed by Monaco and Normand-Cyrot will be analysed. Such a scheme will be shown to be sufficient for providing an adequate discretization for quite large time steps compared to the pseudo-period of the underlying dynamics.

PACS number: 05.45.Pq

## 1. Introduction

Usually physical processes are modelled by differential equations where the processes are assumed to be evolving continuously. But all measurements are available in the form of a time series discretized in time. It is therefore natural to express a model for this measurement with difference equations. Indeed, there are two types of global modelling techniques based on derivative and delay coordinates, respectively. Starting from the phase portrait reconstructed using derivative coordinates, ordinary differential equations are thus obtained [1]. When delay

  

coordinates are used, difference equations are obtained under the form of a nonlinear auto-regressive moving average model [2]. These two types of models may be proposed for the same underlying dynamics. It is therefore relevant to understand deeply the relationships which may exist between difference and differential equations for the same underlying dynamics.

The first step for such a purpose is thus to obtain discretization of the continuous system, the discretization having a solution equivalent to the discrete counterpart. The simplest method for achieving this is to apply an Euler discretization scheme. However, the resulting solution is affected by the choice of the discretization time step. For instance, Lorenz showed that the discretization of a two-dimensional continuous system may generate chaotic behaviour when the time step is sufficiently large [3]. It is known that this type of behaviour cannot be exhibited by the continuous counterpart according to the Poincaré–Bendixson theorem. A one-dimensional difference equation such as the logistic map can also exhibit chaotic solution for large time steps while its continuous counterpart cannot [4]. Although such results are correct, an important point is very often overlooked: these spurious solutions of the discretization scheme which do not correspond to any expected solution of the continuous systems occur for values of the time step outrageously large when compared to the value of the characteristic time scale of the original dynamics. When the time step is sufficiently smaller than the characteristic time scale, we will show that 'unexpected' solutions generated by the discretized model are topologically equivalent to solutions of the continuous counterpart but with a displacement in the parameter space. Such a displacement in the parameter space is also observed when a discrete model is identified directly from a single scalar time series [5]. In this latter case, the reason for such a displacement seems to be the presence of many sources of uncertainty that can be part of the identification procedure. In this paper, the reason is in the discretization scheme itself and therefore could be considered as a general property of discretized dynamical systems.

In order to have a discretization scheme sufficiently robust against increase of the time step, we will use a discretization scheme introduced by Monaco and Normand-Cyrot [6, 7]. Since relatively large sampling time (time step) can be used for estimating a global discrete model, it is important to understand how a discretization depends on the time step. The basic idea behind Monaco and Normand-Cyrot's method is to use a truncated Lie expansion of the differential equation which represents the continuous nonlinear system. It has been shown that such a discretization scheme preserves the fixed points of the continuous system for any order [8] and that the spurious fixed points depend on the time step when higher-order discretized models are considered. In this paper, we will show that Monaco and Normand-Cyrot's scheme is particularly useful when large time steps are considered.

The subsequent parts of this paper are organized as follows. Section 2 briefly describes Monaco and Normand-Cyrot's scheme. In section 3, the dynamical system used as a benchmark is described as well as the typical behaviour which may be observed. Section 4 is devoted to the first four orders of Monaco and Normand-Cyrot's scheme and how increasing the order of the Lie expansion helps in improving the quality of the discretization model. Section 5 gives a conclusion.

## 2. The Monaco and Normand-Cyrot discretization scheme

Consider a dynamical system

$$\dot{\boldsymbol{x}} = \boldsymbol{f}(\boldsymbol{x}) \tag{1}$$

where $\boldsymbol{x} \in \mathbb{R}^m$ is the vector made of the dynamical variables and $\boldsymbol{f}$ are analytic functions of appropriate dimension. The aim is to obtain a discretization of equation (1) for a relatively large value of the discretization time step $h$. Such a discretization reads

$$\boldsymbol{x}_{k+1} = \boldsymbol{g}(\boldsymbol{x}_k, h) \tag{2}$$

where $\boldsymbol{x}_k \in \mathbb{R}^m$ are the dynamical variables at time $t = t_0 + kh$. $h$ is the discretization time step. In order to compute such a discretization, we will use the discretization scheme introduced by Monaco and Normand-Cyrot [6, 7] based on a Lie expansion of equation (1) as follows:

$$\boldsymbol{x}_{k+1} = \boldsymbol{x}_k + \sum_{n=1}^{\eta} \frac{h^n}{n!} \mathcal{L}_{\boldsymbol{f}}^n(\boldsymbol{x}_k) \tag{3}$$

where $\eta$ is the order of the expansion. The Lie derivative is given by

$$\mathcal{L}_{\boldsymbol{f}}(\boldsymbol{x}_k) = \sum_{j=1}^{m} f_j \frac{\partial \boldsymbol{x}}{\partial x_j} \tag{4}$$

where $f_j$ designates the $j$th component of the vector field. The higher order derivatives are given recursively

$$\mathcal{L}_{\boldsymbol{f}}^n(\boldsymbol{x}_k) = \mathcal{L}_{\boldsymbol{f}}\big(\mathcal{L}_{\boldsymbol{f}}^{n-1}(\boldsymbol{x}_k)\big). \tag{5}$$

We will show that such a Lie expansion (3) can be truncated at order $\eta$ to avoid an excessive number of terms. The dependence of the robustness of the discretization versus time step increase will be investigated up to $\eta = 4$. The series truncated at the first order ($\eta = 1$) corresponds to the Euler scheme. In that case, it was shown that the discretization model of first order obtained using the Monaco and Normand-Cyrot's scheme preserves the number and location of fixed points of its original continuous counterpart [8]. For any higher-order discretization ($\eta > 1$), the location of fixed points of the continuous counterpart is preserved but the location and number of spurious fixed points introduced by the higher-order terms depend on the discretization time step $h$.

## 3. The dynamical model

We choose to apply the discretization scheme to the system introduced by Genesio and Tesi in [9] and represented by the following differential equation:

$$\dddot{x} + a\ddot{x} + b\dot{x} + x(1 + x) = 0 \tag{6}$$

which may be rewritten as a set of ordinary differential equations under the form:

$$\begin{cases} \dot{x} = y \\ \dot{y} = z \\ \dot{z} = -az - by - x(1 + x) \end{cases} \tag{7}$$

where $a$ and $b$ are the bifurcation parameters. This system has two fixed points; one, $F_0$, is located at the origin of the phase space and the other, $F_1$, is located at $(-1, 0, 0)$. Fixed point $F_0$ is a saddle-focus with two complex conjugated eigenvalues with positive real parts and $F_1$ is also a saddle-focus but with complex eigenvalues with negative real parts. Such a configuration with two fixed points is very similar to the configuration of the Rössler system [10]. As for this latter system, the asymptotic behaviour settles down to a limit cycle or a chaotic attractor as long as the trajectory does not cross the boundary of the attraction basin associated with the stable manifold of fixed point $F_1$ [11]. Indeed, as soon as the trajectory

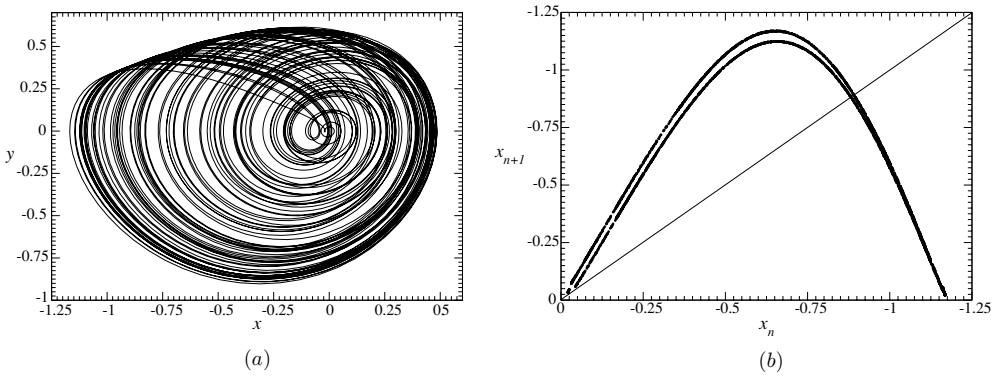


**Figure 1.** Chaotic behaviour solution of system (7) with $a = 0.446$ and $b = 1.1$. ($a$) Phase portrait, ($b$) first-return map.

crosses this manifold, it is ejected to infinity by the unstable manifold corresponding to fixed point $F_1$. A typical chaotic attractor solution of system (7) is shown in figure 1($a$).

A first-return map to a Poincaré section for the system described in equation (7) was computed as shown in figure 1($b$). This is a parabola with a layered structure resulting from the small damping rate of the dynamics. The damping is not sufficient to fully squeeze the folding in one cycle around the fixed point $F_0$. Such a feature is very characteristic of low dissipative systems. Nevertheless, the dynamics remains very similar to the characteristic dynamics of the class defined by the logistic map. Thus, a period-doubling cascade is observed in the bifurcation diagram as well as many periodic windows (figure 5). Basically, after the period-doubling cascade, system (7) may generate a *spiral* attractor associated with a map mainly constituted by one increasing and one decreasing branches.

When the system has a three-dimensional phase space, it is possible to describe the flow by a two-dimensional branched manifold where the two dimensions describe the direction of the flow and the direction of stretching. The number of branches of the template is equal to the number of branches in the first-return map. In the present case, the topological analysis reveals that the layered structure of the first-return map is not relevant and that the map may be considered as made of two branches. Thus, the critical point located at the maximum of the first-return map defines a partition of the phase portrait into two regions. A symbol is associated with each branch. Chaotic trajectories and the periodic orbits constituting their skeleton are thus encoded over the symbol set $\{0, 1\}$. The symbol '0' is associated with the increasing branch and symbol '1' with the decreasing branch. The increasing branches are preserving order and decreasing branches are reversing order [12]. The phase portrait is necessarily divided into one preserving order strip and one reversing order strip. A preserving order strip represents an even number of half-turns while a reversing order strip represents an odd number of half-turns. Consequently, the corresponding template will be composed of two strips. Periodic orbits may thus be encoded by symbolic strings. For instance, a period-2 orbit having one intersection with the Poincaré section located on the branch '0' and one located on the branch '1' is designated by the sequence (10). A period-3 orbit would have three symbols, and so on. The population of periodic orbits embedded within the attractor solution of system (7) is reported in table 1.

An adequate template must predict topological invariants such as linking numbers between pairs of periodic orbits. A periodic orbit is here considered as a knot. Periodic orbits embedded within the attractor can be approximated by segments of the chaotic time series that mimic the

**Table 1.** Population of periodic orbits for system (7). Only orbits with a period smaller than 7 are reported. Parameter values: $a = 0.445$ and $b = 1.1$.

| Orbit | Orbit | Orbit |
|---|---|---|
| 1 | 100 | 100010 |
| 10 | 100101 | 100011 |
| 1011 | 10010 | 10001 |
| 101110 | 10011 | 10000 |
| 101111 | 100111 | 100001 |
| 10111 | 100110 | 100000 |
| 10110 | 1001 | |
| 101 | 1000 | |

behaviour of nearby unstable periodic orbits. A 'close return' method [11] is applied to the Poincaré section to extract them.

The linking numbers are ambient isotopy invariant defined as follows:

**Definition 3.1.** *Let $\alpha$ and $\beta$ be two knots defining a link L in $\mathbb{R}^3$. Let $\sigma$ denote the set of crossings of $\alpha$ with $\beta$. Then the linking number reads:*

$$lk(\alpha, \beta) = \frac{1}{2} \sum_{p \in \sigma} \epsilon(p) \tag{8}$$

*where $\epsilon$ is the sign of each crossing p with the usual convention, that is*

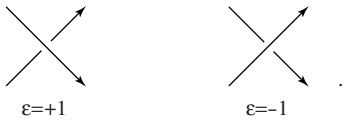


The linking number $lk(\alpha, \beta)$ of two periodic orbits $\alpha$ and $\beta$ is half of the algebraic sum of all crossings between $\alpha$ and $\beta$ (ignoring self-crossings). In practice, the linking numbers are counted on plane regular projections of orbit pairs by using the third coordinate to define the sign of the crossings. For instance, orbits (10) and (101) are depicted in figure 2. This example is very simple and the linking number is found to be equal to $-2$ since five negative and one positive crossing are identified.

All the linking numbers between orbits embedded within the attractor are well predicted by the template (figure 3) where periodic orbits (10) and (101) are drawn. Five negative and one positive crossings are identified. The linking number $\tilde{lk}(10, 101)$ predicted by the template is thus $-2$ as for the plane projection of orbits shown in figure 2. Such a template can be described by the linking matrix

$$M_{ij} = \begin{bmatrix} 0 & -1 \\ -1 & -1 \end{bmatrix} \tag{9}$$

according to the standard insertion convention [13]. The diagonal elements $M_{ii}$ are equal to the number of $\pi$-twists of the $i$th strip and off-diagonal elements $M_{ij}$ $(i \neq j)$ are given by the algebraic number of intersections between the $i$th and $j$th strips. Further details for such a topological characterization procedure are extensively discussed in [14, 11, 15].

Before the boundary crisis producing the ejection of the trajectory to infinity, the *funnel* chaotic attractor (figure 4(*a*)) is characterized by a map with additional branches. A first-return map of up to five branches has been identified in this system (figure 4(*b*)). Such a scenario

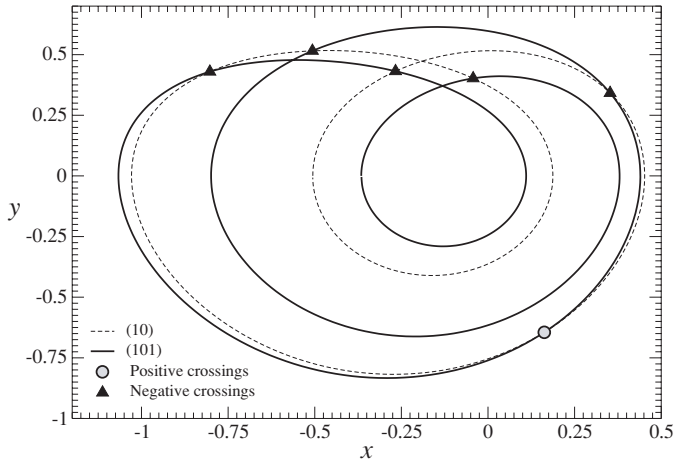


**Figure 2.** A link made of two periodic orbits encoded by (10) and (101), respectively. Five negative and one positive crossings are identified. The linking number $lk(10, 101)$ is therefore equal to $-2$.

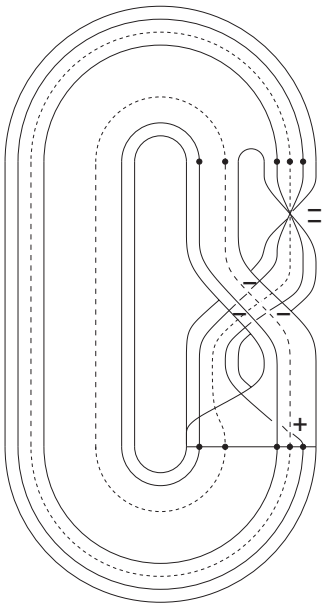


**Figure 3.** Template of the spiral attractor solution of system (7). Periodic orbits (10) and (101) are represented. From this template, the linking number $\tilde{lk}(10, 101)$ is equal to $-2$.

was also observed in the Rössler system although its first-return map may present more numerous branches [11]. Note that the first-return map shown in figure 4(*b*) presents a spurious discontinuity located in the first decreasing branch. This feature results from the fact that the attractor does not present a hole in its middle which could ensure we could properly compute the Poincaré section. This effect is amplified by the low damping rate of the dynamics. The discontinuity is indeed an artefact of our computation of the Poincaré

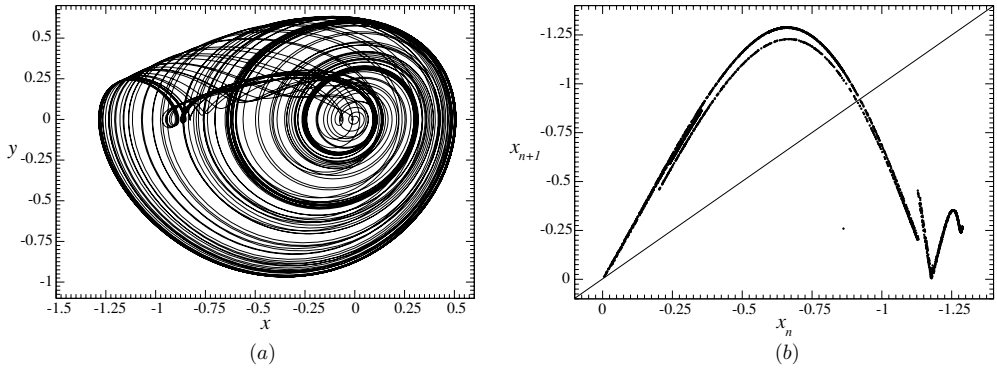


**Figure 4.** Funnel chaotic attractor solution of system (7) with $a = 0.4154$ and $b = 1.1$. ($a$) Phase portrait, ($b$) first-return map.

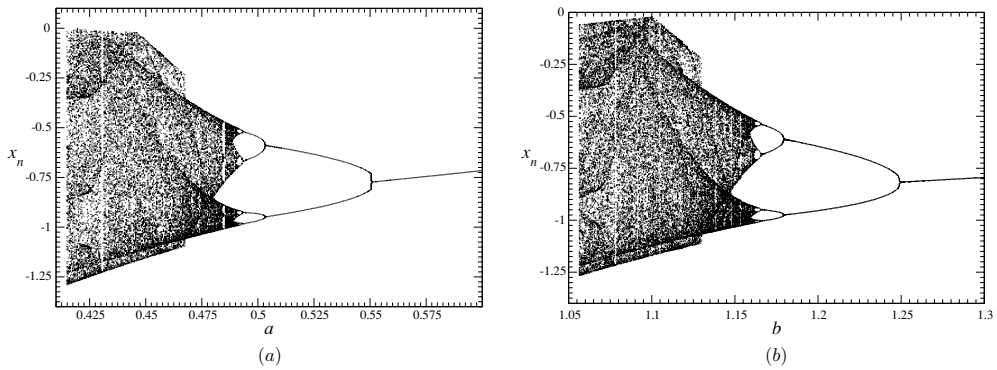


**Figure 5.** Bifurcation diagrams of system (7). The period doubling as a route to chaotic attractor ensures us that the spiral attractor corresponds to the class of chaotic behaviour associated with the logistic map. ($a$) Versus $a$ with $b = 1.1$, ($b$) versus $b$ with $a = 0.446$.

section and these two decreasing branches must be counted for a single branch. The template characterizing this funnel attractor is described by the linking matrix

$$M_{ij} = \begin{bmatrix} 0 & -1 & -1 & -1 & -1 \\ -1 & -1 & -2 & -2 & -2 \\ -1 & -2 & -2 & -3 & -3 \\ -1 & -2 & -3 & -3 & -4 \\ -1 & -2 & -3 & -4 & -4 \end{bmatrix}. \tag{10}$$

Note that this matrix contains matrix (9).

In order to have a global view of the solutions of system (7), bifurcation diagrams are computed versus control parameters (figure 5). In both cases, an inverse period-doubling cascade is observed. The similarities between these two bifurcation diagrams reveal that the parameter space is organized like an onion, that is, the same solution may be observed for many control parameter values located on a surface organized like concentric spheres.

The characteristic frequencies of the spiral and funnel attractors are exhibited by computing two Fourier spectra (figure 6($a$)). The main frequency is observed at $f_0 \approx 0.17$ Hz and therefore corresponds to a pseudo-period equal to 5.9 s. A second frequency clearly

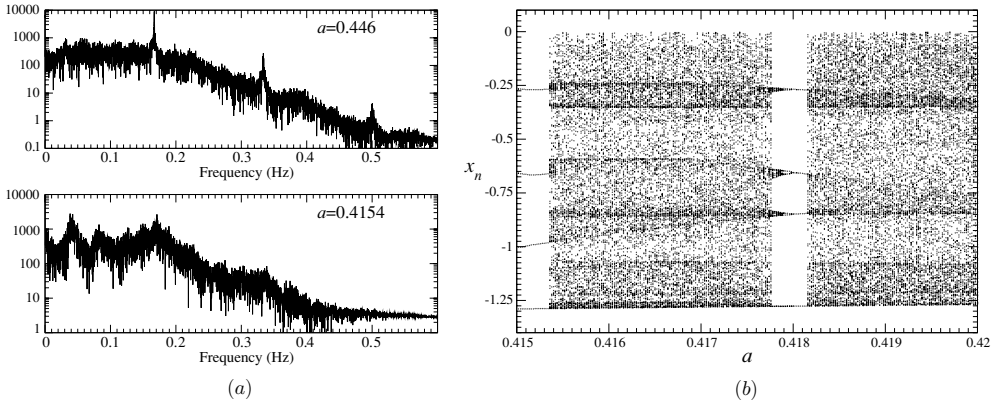


**Figure 6.** Fourier spectra (*a*) for chaotic solutions of system (7) with $b = 1.1$. One main frequency at $f_0 \approx 0.17$ Hz is identified. The frequency $f_0/4$ results from the periodic window associated with a period-4 limit cycle which may be identified under slight change in the bifurcation parameter (*b*). (*a*) Fourier spectra, (*b*) bifurcation diagram.

appears for the funnel attractor ($a = 0.4154$). This is the signature of a periodic window associated with a stable period-4 limit cycle which is identified under a slight change in the bifurcation parameters, $a = 0.418$ for instance (figure 6(*b*)). Note, however, that the boundary crisis that occurs during the second period-4 window can be observed around 0.415.

## 4. Different order approximation schemes

In this section four different discretized models obtained by applying Monaco and Normand-Cyrot's scheme to the system described in section 3 are analysed as the time step is increased.

### *4.1. First-order discretized model*

Applying Monaco and Normand-Cyrot's scheme to system (7) leads to

$$\begin{cases} x_{k+1} = x_k + hy_k \\ y_{k+1} = y_k + hz_k \\ z_{k+1} = z_k - h(az_k + by_k + x_k(1 + x_k)). \end{cases} \tag{11}$$

For sufficiently small time step $h$, the solution of this discretization is topologically equivalent to the attractor solution of continuous system (7). This means that the attractor is characterized by the same template as the spiral attractor of the continuous counterpart. Only the population of periodic orbits is slightly changed. Nevertheless, as usually observed for any type of discretization scheme, the nature of the solution depends on the value of the discretization time step $h$. In order to have a global overview of these solutions, a bifurcation diagram is computed versus $h$ (figure 7(*a*)). The discretization time step may be varied over the range $]0; 0.0358]$. For larger values, the trajectory is ejected to infinity. Over this range, discretized model (11) exhibits either a chaotic attractor or a limit cycle. It has been verified that the chaotic attractors can be described by the template defined by the linking matrix of equation (10). The largest value of the discretization time step corresponds to $\frac{T_0}{165}$, which is a particular small value. Note that the period-4 window is here clearly observed with $h \approx 0.035$ s in the bifurcation diagram (figure 7(*a*)). The boundary crisis therefore occurs in

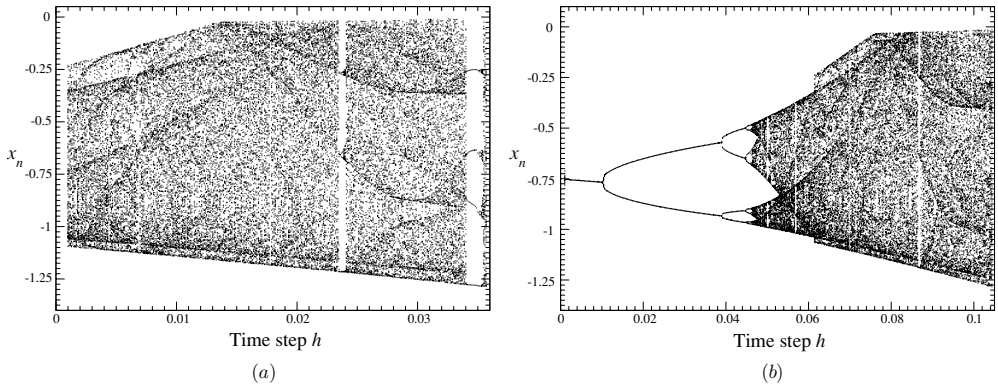


**Figure 7.** Bifurcation diagram versus the discretization time $h$. ($a$) $a = 0.469$ and $b = 1.1$, ($b$) $a = 0.570$ and $b = 1.1$.

conditions very similar to those of system (7). The discretization time step therefore plays the role of one bifurcation parameter. In this case, increasing $h$ is similar to decreasing the parameter $a$. In other words, $h$ plays more or less the same role as the bifurcation parameter $a$. Consequently, all solutions of the discretization of system (7) are topologically equivalent to solutions of its continuous counterpart. The discretization scheme, even for the first order, is already very efficient as long as only the nature of the solution is considered and for sufficiently small value of the discretization time step.

When the highest value of the discretization time step is considered ($h = 0.358$ s), the funnel attractor is observed with $a = 0.469$. The spiral attractor can be recovered when the $a$ bifurcation parameter is changed to 0.504. This is just a consequence of the interplay between the time step $h$ and the bifurcation parameter $a$. Indeed, the effect of the discretization time step $h$ can be balanced by an action on the $a$ parameter value. Such a feature was also observed in a discretization of the Rössler system using nonstandard Mickens' schemes [16]. Applying such a change in the bifurcation parameters allows us to recover the period-doubling cascade which is not observed in the bifurcation diagram computed with $a = 0.469$ and $b = 1.1$ (figure 7($a$)). Choosing $a = 0.570$ with $b$ unchanged, the bifurcation diagram versus the discretization time step presents the period-doubling cascade (figure 7($b$)) as observed in the original system (figure 5). Note that in this case, the time step can be increased up to 0.1046, that is, over a range roughly three times larger than for the original values of the bifurcation parameters.

The topology of the attractor solution of the first-order discretization is investigated for different values of $h$. When $a = 0.469$ and $b = 1.1$, the spiral attractor is obtained until $h$ is smaller than 0.012 s. For this value, the first-return map is made of two monotonic branches (figure 8($a$)). With larger values of $h$, a third branch occurs and the funnel attractor is observed. With $h = 0.012$ s, the population of periodic orbits embedded within the attractor is the same as the population extracted from system (7) with $a = 0.446$ and $b = 1.1$ (compare the first-return maps shown in figures 8($a$) and 1($b$)). The linking number $lk(10, 101)$ is equal to $-2$ as observed for the spiral attractor solution of system (7) (compare figures 8($b$) and 2). This topological equivalence between the first-order discretized model and system (7) may be obtained for any other value of $h$ if the $a$ value for system (7) is properly tuned (a change of the time step in the discrete model can be balanced by a change of the $a$ parameter value).

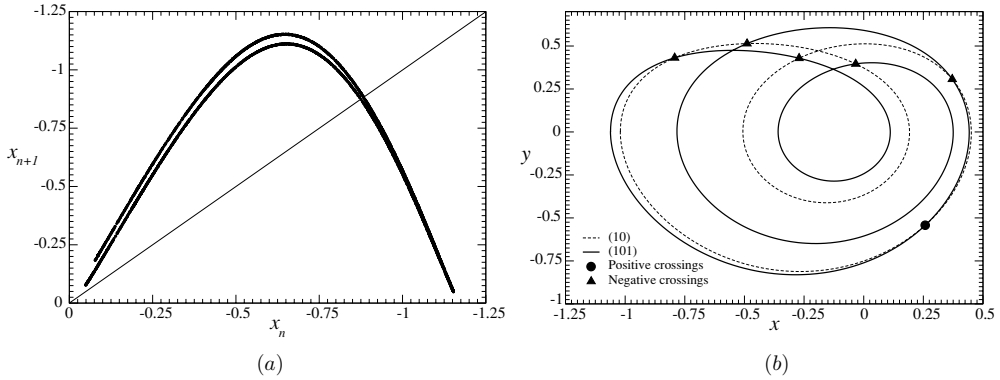


**Figure 8.** First-return map to a Poincaré section of the attractor solution of the first-order discrete model with $a = 0.469$, $b = 1.1$ and $h = 0.012$ s. The link made of periodic orbits (10) and (101) shows that the linking number $lk(10, 101)$ is left unchanged, that is equal to $-2$. (*a*) First-return map, (*b*) orbits (10) and (101).

### *4.2. Second-order discretized model*

The second-order discretization of system (7) is now considered. It reads

$$\begin{cases} x_{k+1} = x_k + hy_k + \frac{h^2}{2}z_k \\ y_{k+1} = y_k + hz_k - \frac{h^2}{2}(az_k + by_k + x_k(1 + x_k)) \\ z_{k+1} = z_k - h(az_k + by_k + x_k(1 + x_k)) \\ \quad - \frac{h^2}{2}[(1 + 2x_k)y_k + bz_k - a(az_k + by_k + x_k(1 + x_k))]. \end{cases} \tag{12}$$

The first obvious advantage presented by this second-order discretization is that the discretization time step may be varied over the larger range ]0; 0.4733]. The largest time step now corresponds to $\frac{T_0}{12}$. More than a factor ten is gained with this second order. Such a feature shows the efficiency of Monaco and Normand-Cyrot's scheme. Indeed, most of discretization schemes found in the literature cannot provide discretized models which remain valid over a very large range of time step $h$. It should also be noted that when the discretization time step is less than 0.1, the bifurcation diagram does not show too many changes in the chaotic behaviour. This means that over this interval, the dynamics is rather not sensitive to increase in the time step $h$. When discretized model (12) is iterated with the largest time step $h = 0.473$ s, 12 points are obtained per cycle. This can be considered as a threshold below which an accurate description of the structure of the attractor is no longer achieved. For instance, to perform topological analysis as developed in [11], an interpolation must be used for extracting the periodic orbits with sufficient accuracy.

When the $a$ bifurcation parameter is changed to 0.560, the bifurcation diagram then presents the period-doubling cascade observed in the original system given by equation (7). The largest discretization time step is equal to 0.723 s, that is $\frac{T_0}{8}$. Such a value for the time step does not allow us to have accurate structure of the dynamics as seen in the bifurcation diagram (figure 9(*b*)). Note that the period-4 window observed for $h \approx 0.62$ s can no longer be detailed nor can the period-doubling cascade occurring in the beginning of this window be identified. It could be considered that the time step $h$ for which a discretized model of the continuous system is no longer adequate has already been achieved. The aforementioned value of $h$ is quite close to the time associated with the Nyquist criterion which states that, when the sampling rate is lower than twice the highest significative frequency in the power spectrum, insufficient information is available for a safe description of the dynamics. In the present case,

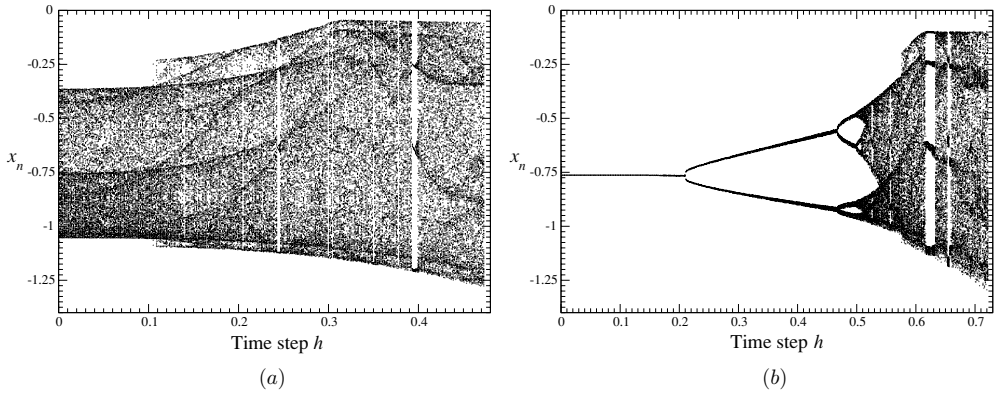


**Figure 9.** Bifurcation diagrams of the second-order discretization versus the time step $h$. $(a)$ $a = 0.469$, $(b)$ $a = 0.560$.

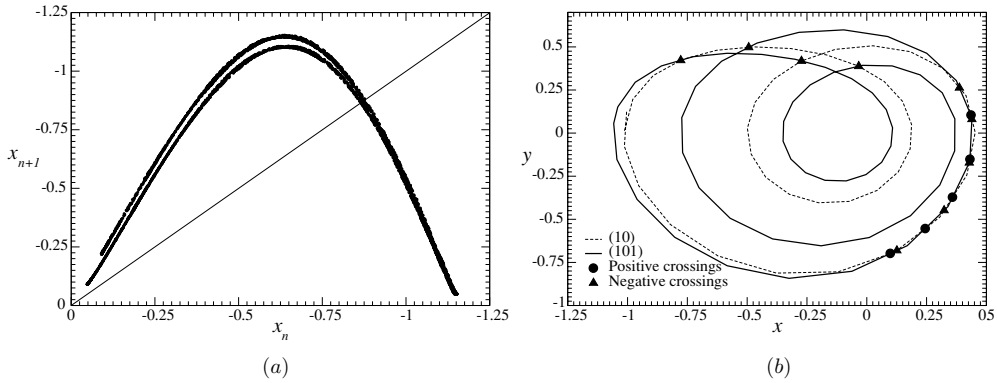


**Figure 10.** First-return map to a Poincaré section of the attractor solution of the second-order discrete model with $a = 0.469$, $b = 1.1$ and $h = 0.31$ s. The link made of periodic orbits (10) and (101) shows that the linking number $lk(10, 101)$ is left unchanged, that is equal to $-2$, although spurious crossings due to the low sampling effect are present. $(a)$ First-return map, $(b)$ orbits (10) and (101).

the highest frequency is around 0.5 Hz (figure 6$(a)$). Consequently, a sampling time less than 1 s must be used if a safe description of the dynamics is required. Since the Nyquist criterion is an idealized threshold, a time step around 0.7 s could be considered adequate. Despite all the discussion, the range over which the dynamics remains topologically equivalent can still be improved as explained in the next section.

As for the first-order model, the topology of the attractor solution of the second-order model is investigated for many different values of $h$. With $a = 0.469$ and $b = 1.1$, the spiral attractor is recovered until $h$ is smaller than 0.31 s. Beyond this value of $h$, the attractor is obtained. With $h = 0.31$ s, the two branch first-return map (figure 10$(a)$) is very similar to the map obtained with system (7) for $a = 0.445$ ($b = 1.1$). The population of periodic orbits is also the same as the population reported in table 1. Linking numbers are unchanged as exemplified by the link made of orbits (10) and (101) shown in figure 10$(b)$. The attractor is therefore characterized by the template shown in figure 3. Spurious crossings which were not identified in the previous cases are observed here. They result from the quite large time step

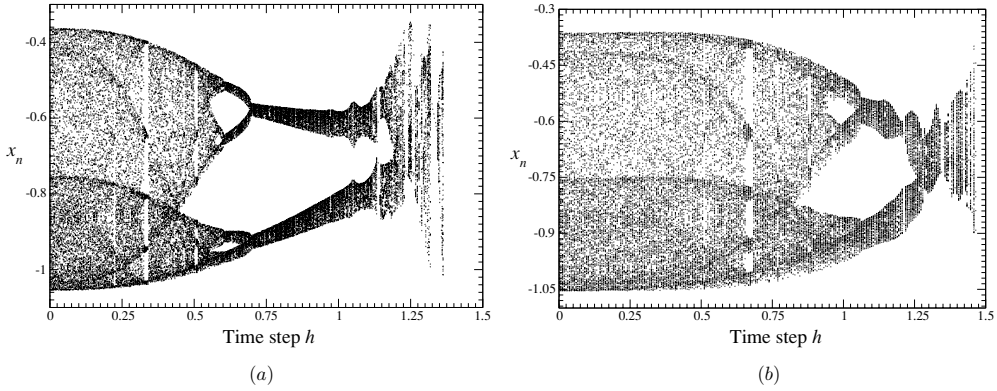


**Figure 11.** Bifurcation diagrams of the third-order ($a$) and fourth-order ($b$) discretizations versus the time step $h$. The control parameters are $(a, b) = (0.469, 1.1)$. ($a$) Third-order discretization, ($b$) fourth-order discretization.

$h$ used. But note that the linking number $lk(10, 101)$ is still equal to $-2$ and, consequently, the topological properties are not affected. These spurious crossings could be deleted by interpolating the data to avoid the low sampling effects.

### *4.3. Third-order discretized model*

We will end this investigation with the third-order discretization of system (7) which reads

$$\begin{cases} x_{k+1} = x_k + hy_k + \frac{h^2}{2}z_k - \frac{h^3}{6}\left(az_k + by_k + x_k + x_k^2\right) \\ y_{k+1} = y_k + hz_k - \frac{h^2}{2}\left(az_k + by_k + x_k + x_k^2\right) \\ \quad + \frac{h^3}{6}\left[-(1+2x_k)y_k - bz_k + a\left(az_k + by_k + x_k + x_k^2\right)\right] \\ z_{k+1} = z_k - h\left(az_k + by_k + x_k + x_k^2\right) + \frac{h^2}{2}\left[-(1+2x_k)y_k - bz_k + a\left(az_k + by_k + x_k + x_k^2\right)\right] \\ \quad + \frac{h^3}{6}\left[(-2y_k + a(1+2x_k))y_k - (ab - 1 - 2x_k)z_k + (a^2 - b)\left(az_k + by_k + x_k + x_k^2\right)\right]. \end{cases} \tag{13}$$

The number of terms becomes quite large but we will show that this discretization provides solutions which are close to the solution of the continuous counterpart for a quite significant interval of the time step. First, the bifurcation diagram (figure 11($a$)) does not look like all diagrams computed for the previous lower order discretizations. In particular, an inverse period-doubling cascade is observed when one of the bifurcation parameters is varied in the original continuous system (figure 5). Consequently, the time step no longer plays the same role as in the previous discretizations. In fact, it now plays a role very similar to the bifurcation parameter $a$ and the dynamics is almost unchanged for values of $h$ up to 0.25 s. For such a value of the discretization time step, around 20 points per cycle are available. This number of points is considered reasonable to accurately describe the topology of the attractor.

Since increasing the value of $h$ no longer corresponds to a development of the dynamics (we observe an inverse period-doubling cascade in the bifurcation diagram shown in figure 11 rather than a direct cascade) and since we would like to check the topology of the phase portrait of third-order discrete model (13) before the transition between spiral and the funnel attractors, the change in $h$ is balanced by a change in $a$ and $a$ must be decreased to recover this transition. The first-return map is thus computed with $a = 0.446$ and $h = 0.31$ s. Again, a two branch map similar to the map for system (7) with the same value of $a$

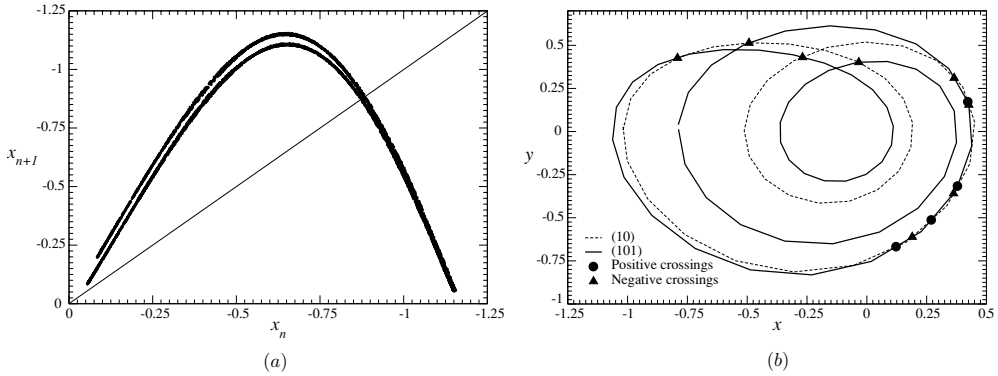


**Figure 12.** First-return map to a Poincaré section of the attractor solution of the second-order discrete model with $a = 0.445$, $b = 1.1$ and $h = 0.31$ s. The link made of periodic orbits (10) and (101) shows that the linking number $lk(10, 101)$ is equal to $-2$, although spurious crossings due to the large time step are present. ($a$) First-return map, ($b$) orbits (10) and (101).

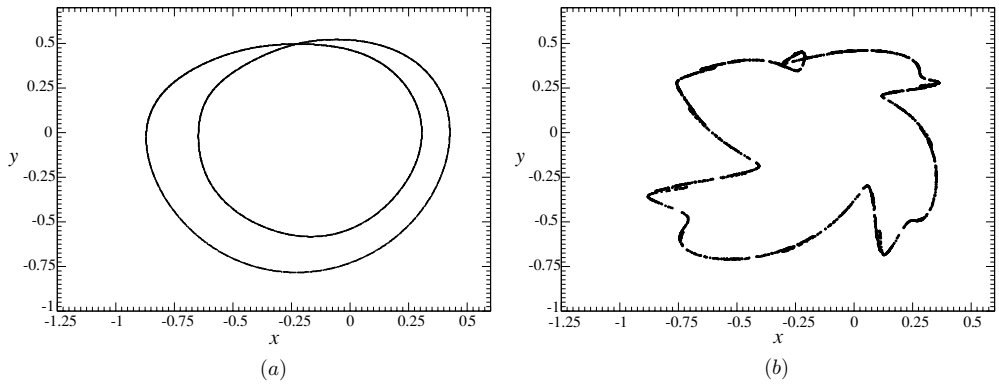


**Figure 13.** Limit cycle generated by the third-order discretization of system (7) for quite large time step. A large number of points are required to obtain a global representation of the dynamics. The continuity can no longer be observed step by step but only with a global point of view. Data points are not connected by segments. ($a$) $h = 1.0$ s, ($b$) $h = 1.25$ s.

(figure 1($a$)) is obtained (figure 12($a$)). The link made of orbits (10) and (101) is shown in figure 12($b$). Spurious crossings are detected due to the large time step but the linking number remains unchanged as for the second-order discrete model (see figure 10($b$)). The population of periodic orbits is the same as for system (7) with the same parameter values. This means that even with a quite large value of $h$, the topology is not affected.

For larger values of the time step ($h \approx 1.0$ s), an inverse period-doubling cascade occurs and ends with a period-2 limit cycle. For such a time step, only six points are available per cycle which is far from enough to have a good representation of the dynamics. Indeed, the continuity of the solution can no longer be obtained step by step but only when quite a large number of iterations are taken into account. In addition to that, the time step is larger than the time associated with the Nyquist criterion. Despite that, the period-2 limit cycle can be reproduced when the points are not joined by straight segments (figure 13($a$)). The blurred aspect of the bifurcation diagram therefore results from the inaccuracy of the Poincaré section and not from the inadequacy of the solution of the third-order discretization. For larger values

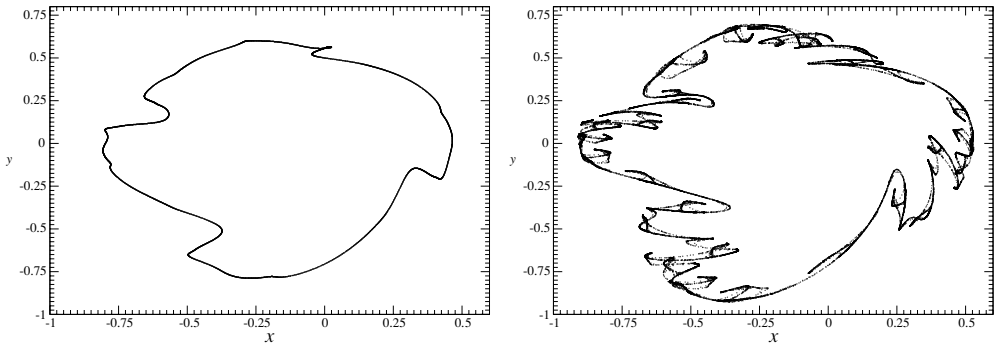


**Figure 14.** Spurious limit cycle (*a*) and chaotic attractor (*b*) observed in the fourth-order discretization of system (7) with two different values of $h$. Remember that these representations are closer to a first-return map to a Poincaré section than to a continuous representation. (*a*) $h = 1.400$ s, (*b*) $h = 1.458$ s.

of the discretization time step, the dynamics is no longer well reproduced as expected. For instance, with $h = 1.25$ s, roughly five points per cycle, the limit cycle observed (figure 13(*b*)) does not have the same configuration as the solution of continuous system (7) would have. Despite its rough appearance, the limit cycle is still topologically equivalent to a circle, that is, to the limit cycle observed with $h = 1.0$ s. It is worth emphasising that the value of the time step is sufficiently large to imply that the discretization becomes quite close to a first-return map to a Poincaré section. Since it is not possible to switch continuously from an attractor to a first-return map, there is necessarily a range of the discretization time step over which the solution cannot correspond to a solution of the continuous system. Therefore, some additional oscillations appear on the limit cycle for sufficiently large $h$. It is important to note that this happens only for time steps larger than the time associated with the Nyquist criterion and consequently the dynamics observed does not correspond to any solution of the original continuous system. This means that with this discretization scheme, the upper limit for the discretization time step is reached.

Using higher order helps a little bit to improve the range over which the time step $h$ is varied without any major bifurcation (figure 11(*b*)). In the case of the fourth-order discretization, not reported here, the time step may be increased up to $h = 0.5$ s without any major modification of the topology of the original attractor. With larger values, periodic orbits are destroyed as seen for the case of the period-5 orbits. These orbits were destroyed just after the window ($h \approx 0.66$ s) where an inverse period-doubling cascade starts leading to the end of the bifurcation diagram. Note that just before the boundary crisis, the behaviour solution of the fourth-order discretization with $h = 1.458$ s is a chaotic attractor (figure 14) and no longer a limit cycle. The route to chaos followed from the period-1 limit cycle to the chaotic attractor is similar to the route described by Lorenz [3], that is, the period-1 limit cycle starts to present a distorted structure as observed in the third-order discretization (figure 13). The boundary crisis occurs sufficiently late to allow the attractor to become chaotic. Obviously, the attractor does not have any topological equivalent in the continuous counterpart. This means that getting a discretization with time step around 1.5 s is no longer an attainable goal since the amount of information required per cycle to describe the structure of the attractor reasonably well is not sufficient. This was expected as the Nyquist criterion was violated and therefore such a discretization should not be attempted.

## 5. Conclusion

We showed that Monaco and Normand-Cyrot's scheme based on a truncated Lie expansion of the differential equation that describes the continuous system under investigation can be used very efficiently to obtain quite accurate discretization of a continuous nonlinear system. This has been checked using a simple system generating chaotic behaviour. It was shown that even with a low-order scheme, the solutions of the discretization are topologically equivalent to some solutions of the continuous counterpart. To recover the original dynamics, the bifurcation parameters must be changed. In other words, applying a discretization scheme necessarily induces a displacement in the parameter space when the discretization time step is greater than a threshold which depends on the order of the discretization used. Using higher-order discretization schemes allows one to obtain difference equations that are able to reproduce the solutions of the original continuous system without any displacement in the parameter space, and for a significant range of time steps. It has been shown that it becomes almost impossible to obtain accurate discretization for time steps greater than the time associated with the Nyquist criterion. This seems reasonable since for larger values the dynamics can no longer be accurately described. Similar results have been observed with discretization of the Rössler system using Mickens' nonstandard scheme and we believe that the features reported here are quite general.

It may be concluded from this investigation that the discretization tends to converge towards a quite stable topology when the third-order or higher-order discretization is used. Using a higher order scheme would improve a little bit the range over which the time step may be varied without any major change in the dynamics, but the significant increase in the number of terms involved may not always justify such a choice. For the majority of cases, it seems that the second-order would be a practical choice due to its rather limited number of terms and its significant range of value for the time step for which the dynamics is reproduced without a too large important displacement in the parameter space.

## Acknowledgments

This work has been partially supported by CNPq and CNRS. We would like to thank L A Aguirre for encouraging this work.

## References

[1] Gouesbet G and Letellier C 1994 Global vector field reconstruction by using a multivariate polynomial $L_2$-approximation on nets *Phys. Rev.* E **49** 4955–72
[2] Billings S A, Chen S and Korenberg J M 1989 Identification of MIMO nonlinear systems using a forward-regression orthogonal estimation *Int. J. Control* **49** 2157–89
[3] Lorenz E N 1989 Computational chaos—a prelude to computational instability *Physica* D **35** 299
[4] Yamaguti M and Matano H 1979 *Proc. Japan. Acad.* **56** 78
[5] Aguirre L A, Letellier C and Maquet J 2002 Induced bifurcations in the validation of nonlinear dynamical models *Int. J. Bifurcation Chaos* **12** 135–45
[6] Monaco S and Normand-Cyrot D 1982 *Proc. 24th Conf. on Decision and Control (Fort Lauderdale)* pp 1457–82
[7] Monaco S and Normand-Cyrot D 1990 A combinatorial approach to the nonlinear sampling problem *Lecture Notes in Control and Information Sciences* vol 144 ed M Thomas and A Wymer (Berlin: Springer) pp 788, 797
[8] Mendes E M A M and Billings S A 2002 A note on discretization of nonlinear differential equations *Chaos* **12** 66–71
[9] Genesio R and Tesi A 1992 *Automatica* **28** 531
[10] Rössler O E 1976 An equation for continuous chaos *Phys. Lett.* A **57** 397–8

[11] Letellier C, Dutertre P and Maheu B 1995 Unstable periodic orbits and templates of the Rössler system: toward a systematic topological characterization *Chaos* **5** 271–82
[12] Bergé P, Pomeau Y and Vidal Ch 1984 *L'ordre dans le chaos* (Paris: Hermann)
[13] Melvin P and Tufillaro N B 1991 Templates and framed braids *Phys. Rev.* A **44** 3419–22
[14] Mindlin G B, Solari H G, Natiello M A, Gilmore R and Hou X J 1991 Topological analysis of chaotic time series data from the Belousov–Zhabotinski reaction *J. Nonlinear Sci.* **1** 147–73
[15] Gilmore R 1998 Topological analysis of chaotic dynamical systems *Rev. Mod. Phys.* **70** 1455–529
[16] Letellier C, Elaydi S, Aguirre L A and Alaoui A Difference equations versus differential equations, a possible equivalence? *Physica* D submitted